Laser-Directed Assembly of Aligned Carbon Nanotubes in Three Dimensions for Multifunctional Device Fabrication

*Wei Xiong, Ying Liu, Li Jia Jiang, Yun Shen Zhou, Da Wei Li, Lan Jiang, Jean-François Silvain, and Yong Feng Lu**

Advanced 3D micro/nanofabrication of functional devices represents a key research topic in modern nanoscience and technology and is critically important in numerous emerging fields, such as micro/nanoelectromechanical systems (MEMS/NEMS),[1] nanoelectronics,[2] micro/nanophotonics,[3] biomedical engineering,[4] bio-inspired architectures,[5] and micro/nanofluidics.[6] Among various existing 3D micro/nanofabrication methods, including nanoimprint lithography,[7] scanning probe lithography,[8] and soft lithography,[9] two-photon polymerization (TPP) based on laser direct writing is regarded as one of the most promising methods due to its unique combination of true 3D fabrication capability and high spatial resolution.[10] An ultrafine line width of ≈40 nm and relatively high fabrication throughput with writing speeds of 1–5 cm s^{-1} have been reported recently.[11] Furthermore, TPP lithography was found to be an ideal tool for developing 3D functional architectures using composite resins doped with various functional materials, including photoisomerizable dyes,[12] semiconductor nanoparticles,[13] metallic nanoparticles,[14] and magnetic nanoparticles.[15] Besides photopolymerization, various other photochemical/photophysical mechanisms can be also used in micro/nanodevice fabrication, including photoisomerization,[16] photoreduction,[17] photo-precipitation of sol–gel,[18] and other novel laser-induced photochemical transformation processes.[19]

Due to their remarkable mechanical, electrical, thermal, and optical properties, carbon nanotubes (CNTs) are promising fillers in polymer-based composites[20] and have already demonstrated remarkable performance enhancements of polymer matrices, including mechanical, electrical, and thermal properties achieved by solution-blended,[21] melt-blended,[22] or in situ polymerization methods.[23] However, the effective utilization of CNTs in composite materials strongly depends on the CNT weight percentage, dispersion quality, and the placement of CNTs throughout the polymer matrix.[24] Precise assembly of CNTs in arbitrary 3D space with proper alignment is critically important and desirable for CNT applications but still remains as a long-standing challenge. Using the TPP technique, it is possible to fabricate 3D micro/nanoscale CNT/polymer architectures with proper CNT alignments in desired directions,[25,26] which is expected to enable a broad range of applications of CNTs in functional devices.

However, three challenges remain in TPP fabrication with CNT-doped composite resins:

1. It is difficult to develop TPP-compatible photoresists with both homogenous CNT dispersion and high CNT concentrations. The strong van der Waals interactions among individual CNTs make them prone to forming large bundles or aggregations rather than uniform dispersion.
2. The linear optical absorption of CNTs significantly limits the maximum doping level of CNTs in the composite resins for nonlinear TPP lithography.[24] TPP-compatible resins with large MWNT concentrations are still lacking.
3. Due to the low concentration of CNTs, the performance enhancement in TPP-fabricated structures is still constrained.[24] Performance demonstration of MWNT/polymer-based functional devices made by TPP lithography is rarely reported.

To unleash the full potential of CNTs, it is strategically important to develop TPP-compatible resins with high CNT concentrations for precise assembly of CNTs into 3D micro/nanostructures for functional device applications.

We investigated a thiol grafting method in functionalizing multiwalled carbon nanotubes (MWNTs) to develop TPP-compatible MWNT-thiol-acrylate (MTA) composite resins. The composite resins developed had high MWNT concentrations up to 0.2 wt%, over one order of magnitude higher than previously published work.[26] Significantly enhanced electrical and mechanical properties of the 3D micro/nanostructures were achieved. Precisely controlled MWNT assembly and strong anisotropic effects were confirmed. Microelectronic devices made of the MTA composite polymer were demonstrated. The nanofabrication method can achieve controlled assembly of MWNTs in 3D micro/nanostructures, enabling a broad range of CNT applications, including 3D electronics, integrated photonics, and MEMS/NEMS.

Dr. W. Xiong, Y. Liu, L. J. Jiang, Prof. Y. S. Zhou, Dr. D. W. Li, Prof. Y. F. Lu
Department of Electrical and Computer Engineering
University of Nebraska-Lincoln
Lincoln, NE 68588-0511, USA
E-mail: ylu2@unl.edu
Dr. W. Xiong
Wuhan National Laboratory for Optoelectronics
Huazhong University of Science and Technology
1037 Luoyu Road, Wuhan 430074, China
Prof. L. Jiang
School of Mechanical Engineering
Beijing Institute of Technology
Beijing 100081, China
Prof. J. F. Silvain
Institut de Chimie de la Matière Condensée de Bordeaux
Avenue du Docteur Albert Schweitzer
F-33608 Pessac Cedex, France

DOI: 10.1002/adma.201505516

Figure 1 illustrates an experimental procedure for preparing MTA composite resins for TPP fabrication. The MTA resins were prepared by directly adding acid-purified MWNT powders of different amounts into homemade TPP-compatible thiol-acrylate resins (see photoresist preparation in the Experimental Section). The dependence of MWNT doping concentration on the MWNT size and morphology was reported by Ntim et al. where they found that shorter MWNTs show smaller particle aggregates with improved MWNT dispersion as compared to longer MWNTs.[27] In our study, longer MWNTs were supposed to form larger aggregates, centrifuged out of the composite resin, thus leading to a lower MWNT loading concentration. Therefore, it is expected that shorter MWNTs may result in better dispersion quality and higher loading concentration for the TPP fabrication. However, a balance on CNT length should be considered since shorter CNTs may result in a reduced electrical conductivity in forming conductive networks embedded inside the polymer matrix.[28] The reasons for choosing pentaerythritol tetrakis (PETMP) and di-trimethylolpropane tetraacrylate (Di-TMPTTA) are their miscibility and branched structures, which favor the formation of highly cross-linked networks. The photoinitiator of 2-Benzyl-2-(dimethylamino)-4′-morpholinobutyrophenone (BDMP) was used due to its high initiation efficiency and large absorbance in the 300–400 nm wavelength range,[29] which is suitable for TPP lithography. The as-prepared resins showed excellent dispersion of MWNTs through the composite resins and had a high stability which could last for one week under ambient conditions without

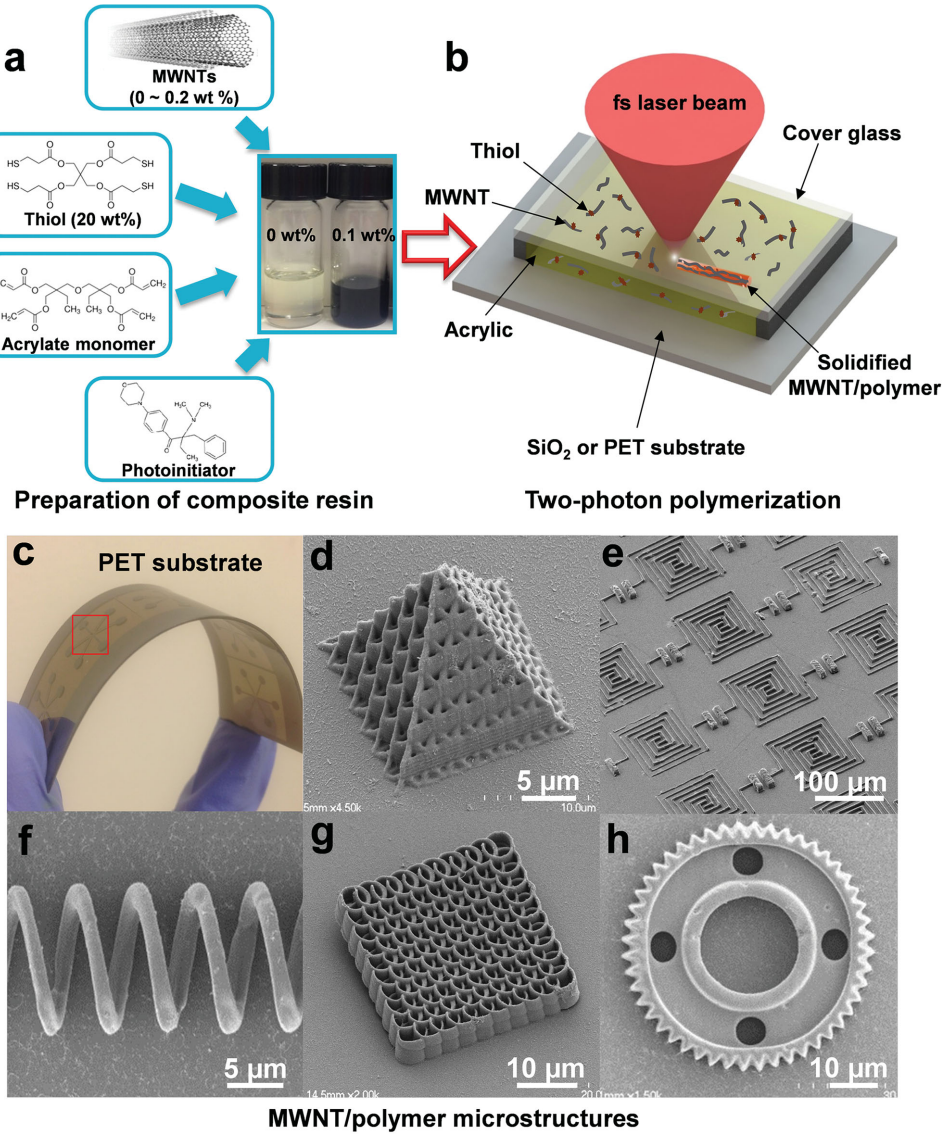

Figure 1. 3D micro/nanofabrication based on MTA composite resins by TPP lithography. a) Experimental procedure in preparing MTA composite resins. b) Experimental setup of TPP fabrication. c) A bent polyethylene terephthalate (PET) substrate used for TPP fabrication with Au electrode patterns. d–h) Scanning electron microscopy (SEM) micrographs of various functional micro/nanostructures including d) a micropyramid, e) arrays of microcapacitors, f) a microcoil inductor, g) a spiral-like photonic crystal, and h) a microgear. The laser power and scanning speed used in the TPP fabrication were 15 mW and 0.5 mm s^{-1}, respectively.

obvious MWNT aggregation (Figure S1a, Supporting Information). In comparison, the MWNT composite resins without thiol molecules degrade in several hours with serious MWNT aggregation resulting in low MWNT concentration, indicating the important role of thiol molecules in MWNT dispersion (Figure S1b, Supporting Information).

Using TPP lithography, a fs laser beam (center wavelength of 780 nm, pulse width of 100 fs, and repetition rate of 80 MHz) was tightly focused into the MTA resin to make 3D scans according to geometric user designs, resulting in solidified 3D micro/nanostructures with MWNTs simultaneously incorporated inside the polymer. After TPP lithography, the samples were developed; and the unsolidified resin was rinsed away, leaving the 3D architectures of MTA composite polymer on the substrates. The TPP fabrication was independent of substrates, which can be conducted on either flexible polyethylene terephthalate (PET) or rigid substrates, including SiO_2/Si, silica, and glass. Electrode patterns were made on the substrates prior to TPP lithography to provide electrical contact with the MWNT-based micro/nanostructures for device fabrication (Figure 1c). Figure 1d–h shows some examples of the 3D microstructures made from the MTA resins, including arrays of microcapacitors, microcoil inductors, spiral-like photonic crystals, micropyramids, and microgears. A broad range of functional micro/nanostructures was easily fabricated via TPP lithography using the MTA composite resins.

Raman spectroscopy was conducted to confirm that the MWNTs were indeed incorporated inside the solidified micro/nanostructures, as shown in **Figure 2**. Characteristic G and D bands of the MWNT fingerprints were observed from the as-fabricated structures (Figure S2 shows the Raman spectra of MTA composite polymers with increased MWNT concentrations from 0 to 0.2 wt%, Supporting Information). Compared with the Raman spectra of pure MWNTs, the slight difference in the line shape and blueshift of the G band of MWNTs in the MTA composite indicate the thiol grafting of MWNTs in the composite resins,[30] which is similar to the previous studies of CNT functionalization with polymers.[31,32] In this work, the thiol molecules are believed to be anchored to the MWNT surfaces, forming covalent functionalization of the MWNTs (Figure S3, Supporting Information). It is reported that the strong attachment of the polymers to CNTs induces the observed blueshift of G band in Raman spectroscopy due to the increase in the elastic constant of the harmonic oscillators of the polymer-coated MWNTs.[32,33] Moreover, the thiol-acrylic polymers provide additional carbon source which may contribute to the defect repairing of the embedded MWNTs during the annealing process, thus leading to a reduced I_D/I_G ratio after thermal annealing of the MTA composite (Figure S4, Supporting Information). A Raman mapping image of a "TPP" pattern fabricated by TPP lithography was obtained using the G-band intensity mapping at each pixel, showing the distribution of MWNTs in the microstructures (Figure 2b). The Raman image matched the scanning electron microscopy (SEM) image of the corresponding structure, indicating that the MWNTs were uniformly distributed throughout the whole structure. Furthermore, due to the large difference in thermal stability between the MWNTs and the polymer, the MWNT distribution inside the composite polymer can be unveiled further by selectively evaporating the polymer components via either laser irradiation

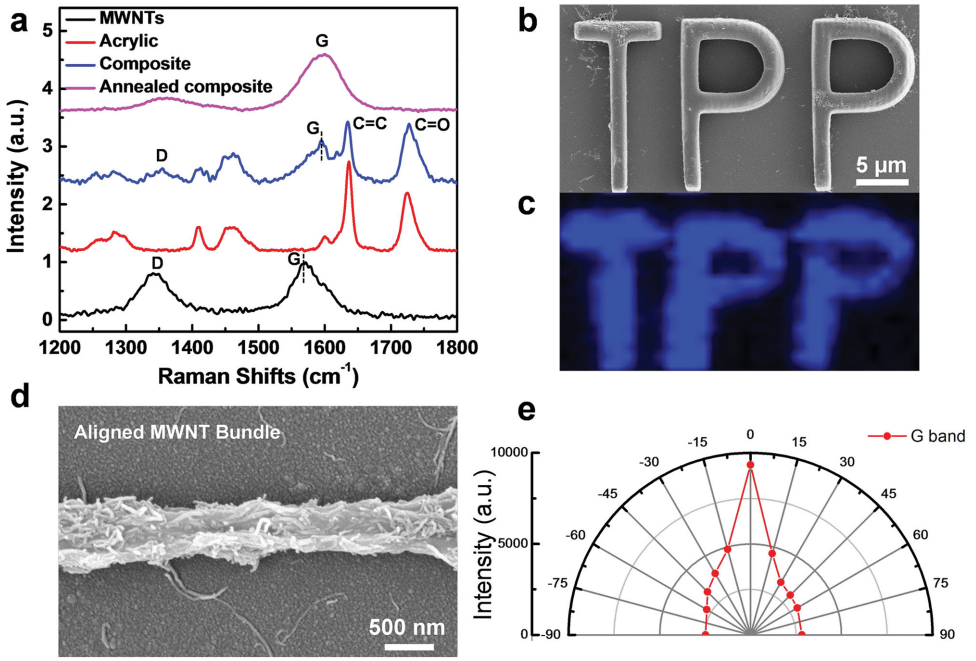

Figure 2. Distribution and alignment of MWNTs inside the MTA composite polymer. a) Raman spectra of MWNTs, acrylate polymer, MWNT/acrylate composite, and annealed MWNT/acrylate composite (500 °C for 5 min). b) SEM micrograph of a "TPP" pattern on a SiO_2/Si substrate. c) Raman mapping image of the corresponding TPP pattern using the G-band of the MWNTs. d) SEM micrograph of a microline structure after thermal annealing at 500 °C for 5 min. e) Polar-diagram showing the G-band intensities as functions of the angle θ between the polarization of the excitation laser used in Raman spectroscopy (514.5 nm) and the wire axis.

or thermal annealing. Figure 2d shows the SEM micrographs of microstructures after 5 min of thermal annealing at 500 °C. It is clear that the MWNTs embedded in the microstructures are aligned in the laser scanning direction during the TPP fabrication. Moreover, the polarized Raman spectroscopy of a straight wire of MTA composite polymer also shows that the G-band peak varies significantly in intensity as a function of θ between the polarization of the incident laser beam used in Raman spectroscopy and the wire axis. The peak intensity of the G-band became strongest when the laser polarization was parallel with the axis of the wires ($\theta = 0$), while the peak intensity became weakest when the laser polarization was perpendicular to the wires ($\theta = 90°$). Both destructive and nondestructive characterization methods confirmed that the MWNT orientations were aligned to the laser scanning direction in the TPP-fabricated microstructures. The major mechanism for the MWNT alignment inside the composite polymer is ascribed to the spatial confinement effect.[25] Since the length of MWNTs was longer than the linewidth of the solidified polymer wires fabricated by TPP, the trapped MWNTs have no way but aligning with the polymer wires in the laser scanning direction. Moreover, the volume shrinkage which resulted in tensile force along wires also contributed to the alignment effect of MWNTs.[25,26] The alignment effect due to the optical gradient forces was minor in this work since the laser beam of our TPP system is in circular rather than linear polymerization.[34]

To characterize the electrical conductivity of the MTA composite polymers, we fabricated two $5 \times 5 \times 75$ μm^3 (W×H×L) bar-shaped channels connecting two pairs of Au electrodes for electrical characterization. Both channels had the same geometry but were fabricated using two different laser scanning directions, either parallel with or perpendicular to the bar axis (**Figure 3**a). The *I–V* curves show that the bar-shaped channel fabricated using parallel scanning was 1000 times more conductive than that fabricated with perpendicular scanning (Figure 3b). The three-orders-of-magnitude difference in electrical conductance matched with the high anisotropy in electrical conductivity of CNTs in directions parallel with or perpendicular to the CNT axis,[35] which further confirms the strong orientation alignment of the MWNTs inside the polymer. Figure 3c shows the electrical conductivity of the MTA composite polymers with respect to different MWNT concentrations. The conductivity of the MTA composite polymer increased drastically with increasing MWNT concentrations from 0 to 0.2 wt%. An increase in the electrical conductivity of over 11 orders of magnitude was observed by loading 0.2 wt% MWNTs into the acrylate-based resins. The average conductivities of MTA composite polymers with 0.15 and 0.2 wt% MWNT concentrations were measured to be 7.54 and 46.8 S m^{-1}, respectively. It is noteworthy that these conductivity values are at least one order of magnitude higher than previously reported results achieved by TPP lithography using either a CNT/polymer composite[24] or a conductive polymer.[36] Highly homogeneous dispersion of relatively large MWNT loadings (at least one order of magnitude larger than refs. [25,26]) within the composite polymers was believed to lead to the superior conductivity of the MTA

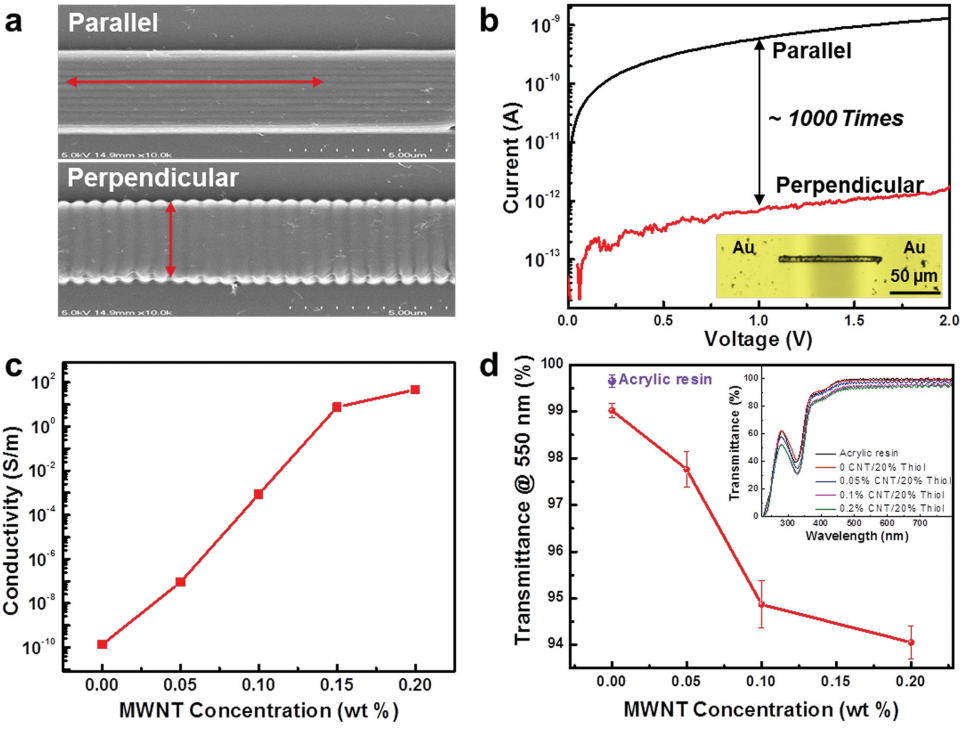

Figure 3. Electrical and optical properties of the MTA composite polymers. a) SEM micrographs of two rectangle bars of identical geometry fabricated using either parallel or perpendicular laser scanning directions with respect to the longer axis of the bars. b) *I–V* curves of both corresponding bars between Au electrodes. The inset shows the optical micrograph of the bridge bar. c) Electrical conductivity of the MTA composites with respect to the MWNT concentrations. d) Optical transmittance of the MTA composite thin films at a wavelength of 550 nm. The inset shows the optical transmittance spectra of the MTA composite thin films.

composite polymers. The high electrical conductivity of the TPP-fabricated structures implies a step forward in TPP fabrication, enabling the realization of arbitrary 3D conductive micro/nanostructures which are desirable for many device applications.

In addition to the electrical properties, we also characterized the optical transparency of the MTA polymers. Figure 3b shows the optical transmittance of the MTA thin films cured by single-photon polymerization using ultraviolet (UV) lithography. As the concentration of MWNTs increased from 0 to 0.2 wt%, the transmittance of the MTA thin films decreased slowly from 99% to 94% at 550 nm, indicating an excellent optical transparency of the MTA composite polymers. Besides the electrical anisotropy, anisotropic optical properties due to the aligned MWNTs with laser-controlled orientation are also expected as evidenced by the characterization results on the polarized transmittance of the aligned CNT/polymer composite.[37] The combination of high optical transmittance, electrical conductivity, and anisotropic properties of the MTA composite polymers is promising for a broad range of optoelectronic applications such as organic solar cells, light-emitting diodes (LEDs), polarization controllers, and integrated optics.

Besides the enhancement of electrical conductivity, the loading of MWNTs was found to significantly enhance the mechanical properties of the TPP-cured polymer structures. We studied the shrinkage of an 8-layer woodpile structure (rod-to-rod distance: 4 μm; layer-to-layer distance: 1.2 μm) fabricated by TPP lithography using the MTA composite resins with different MWNT concentrations. The percent of shrinkage (PS) was gauged by measuring the difference in length between the top layer and the bottom layer of the woodpile structures, as shown in **Figure 4**a. Figure 4b shows that the PS decreased from 4.0% to 2.4% as the MWNT concentration increased from 0 to 0.2 wt%, suggesting that the mechanical strength of the polymer structures is enhanced due to the MWNT reinforcement. Figure 4c,d further demonstrate the enhancement of the mechanical strength by loading the MWNTs. Two suspended microbridges of identical geometric design were fabricated by TPP lithography using pure acrylate (MWNT 0 wt%) and MTA (MWNT 0.1 wt%) resins, respectively. Both microbridges were 2 μm thick and 5 μm wide and were fabricated by scanning a laser beam from one cubic support to another in a layer-by-layer manner. Under the same fabrication conditions (laser power: 30 mW, scanning speed: 10 mm s^{-1}), the bridge made of pure acrylate resin failed to survive the development step and deformed seriously due to the poor mechanical strength of the pure acrylate polymer. In contrast, the microbridge made by the MTA composite remained straight without obvious deformation after the development step, indicating the obvious enhancement in the mechanical strength due to the MWNT reinforcement in the polymer. The nanoindentation testing of a cubic structure fabricated using acrylate and MTA resins also shows different force-displacement behaviors. Higher mechanical strength of the MTA composite polymer was observed as compared with the acrylate polymer, suggesting the MWNT reinforcement effect (Figure S5, Supporting Information).

To demonstrate the potential of TPP fabrication based on the MTA resins (MWNT concentration: 0.1 wt%), we fabricated a series of microelectronic devices, including arrays of capacitors (**Figure 5**a) and resistors (Figure 5c) on SiO_2/Si substrates. We first deposited electrode patterns on the substrates using Au sputtering. The MWNT-based functional microstructures were then fabricated to connect the electrodes via TPP lithography using the MTA composite resins. The performance of the microelectronic devices was measured by an Agilent semiconductor parameter analyzer 4155C and an impedance analyzer 4192A. Figure 5b shows a typical hysteresis loop of the capacitor arrays (containing ten microcapacitors in parallel). The capacitance was measured to be 50 pF.

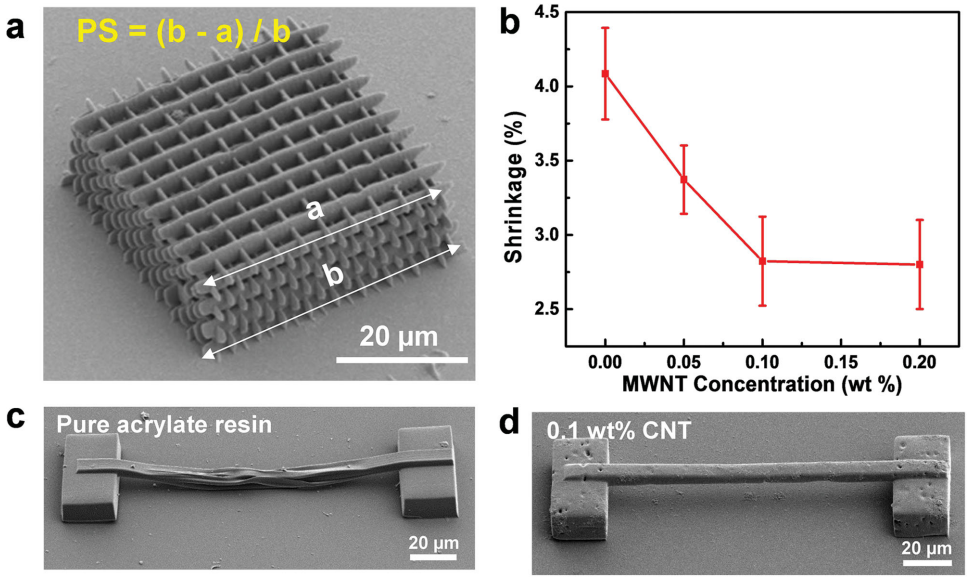

Figure 4. Mechanical properties of the MTA composite polymers. a) SEM micrograph of a woodpile structure fabricated using the MTA composite resin (PS: percent of shrinkage). b) Shrinkage of the woodpile structures as a function of the MWNT concentration. The microbridges fabricated using c) pure acrylic and d) MTA (0.1 wt% MWNTs) resins. The laser power and scanning speed were 30 mW and 10 mm s^{-1}, respectively.

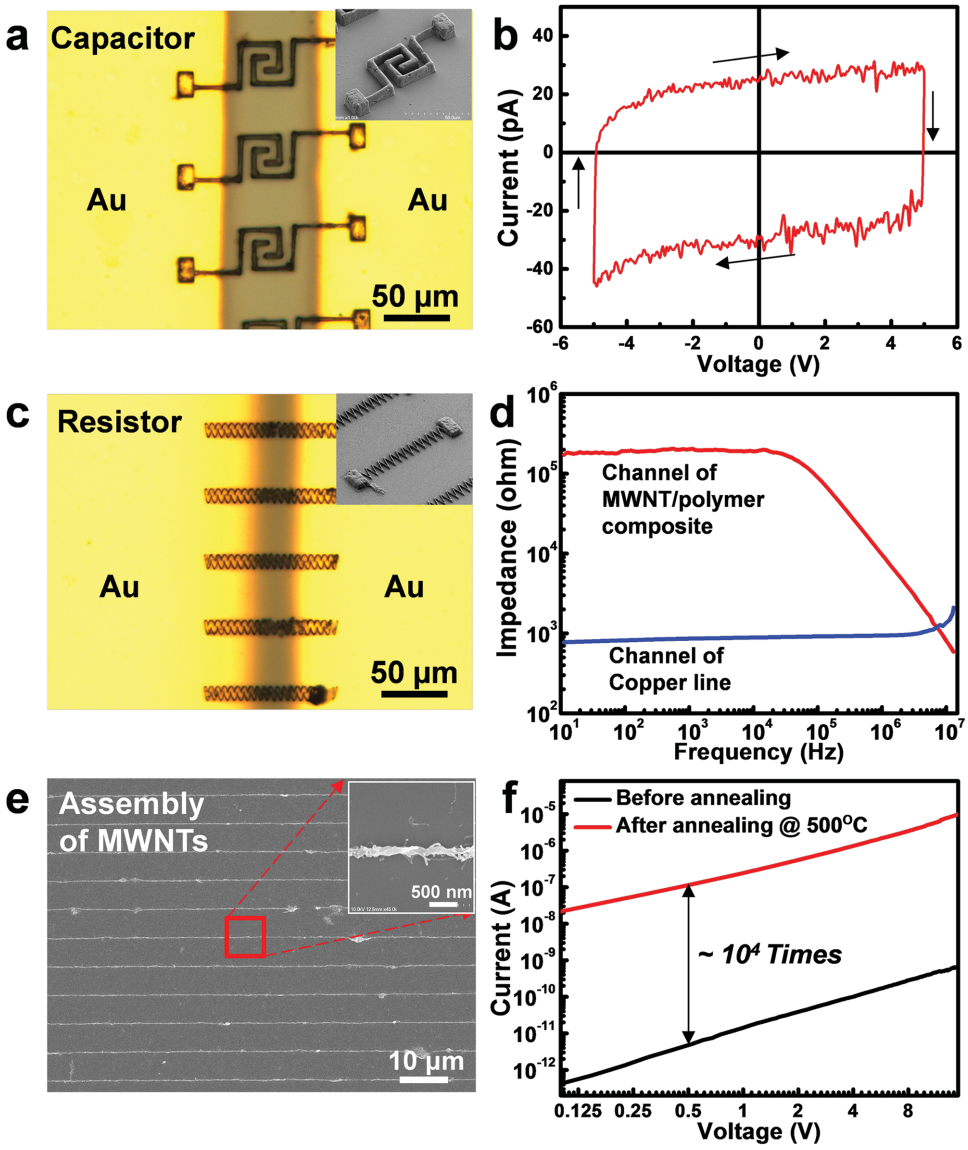

Figure 5. TPP fabrication of MWNT-based functional structures for electronic applications. a) Optical micrograph of a capacitor array between two Au electrodes. The inset shows the SEM micrograph of a single capacitor. b) Hysteresis loop of the capacitors (scanning frequency at 0.025 Hz). c) Optical micrograph of an array of zigzag resistors. The inset shows the SEM micrograph of a single zigzag resistor. d) Frequency responses of transmission lines made of MTA composite (MWNT 0.1 wt%) and copper (length × width × thickness: 1 cm × 5 μm × 50 nm, fabricated by Cu sputtering with a shadow mask) as a reference (4192A Impedance Analyzer, Hewlett-Packard, frequency coverage is 5–13 MHz). e) SEM micrograph of parallel lines of MWNTs assembled on a SiO_2/Si substrate after thermal annealing (500 °C for 5 min in vacuum). The inset shows the zoomed-in SEM micrograph of an assembled MWNT bundle. f) *I–V* curves of a two-terminal device containing ten parallel MTA polymer lines assembled between two electrodes before and after the thermal annealing (500 °C for 5 min in vacuum).

Figure 5d shows the frequency responses of transmission lines made by MTA composite polymer (containing 20 zigzag microresistors in parallel) and copper micro-ribbon (length × width × thickness: 1 cm × 5 μm × 50 nm, fabricated by Cu sputtering with a shadow mask). In the low frequency range, from 0 to 100 KHz, both MTA polymer and Cu transmission lines exhibited relatively stable AC impedances of ≈90 KΩ (MTA polymer) and ≈900 Ω (Cu), respectively. However, in the high frequency range, above 100 KHz, the two transmission lines showed different frequency responses. For the Cu transmission line, due to the increasing skin effect at high frequency, the impedance of the transmission line increased from ≈900 (100 kHz) to 1356 Ω (10 MHz). In contrast, the impedance of the MTA polymer transmission lines decreased exponentially from 90 000 (100 kHz) to 808 Ω (10 MHz), even lower than that of the Cu transmission line at a frequency of >8 MHz. Figure 5d suggests that the MTA composite has an excellent electrical conductance at high frequency, which is ascribed to the effective mitigation of the skin effect by the MWNTs.[38] It is expected that the electrical devices based on the MTA composite polymer are promising for various high frequency applications including RF electronics.

Besides the characterization of the microdevice based on the MTA composite polymer, we also studied the influence of the thermal annealing process on the electrical performance of the MTA polymer-based resistors. By selective thermal evaporation of the polymer component out of the MTA composite, the electrical conductance of the channels increased significantly. An increase in electrical conductance of over four orders of magnitude was observed after 5 min of thermal annealing at 500 °C in vacuum (Figure 5f). Interestingly, the remaining MWNT bundles on substrates were deposited at the same location, as defined by TPP fabrication before annealing. Hence, a tightly controlled MWNT assembly has been realized by the TPP fabrication followed by a simple thermal annealing. The MWNT assembly method has numerous advantages, such as user-defined CNT placement (arbitrary CNT patterns), well controlled CNT orientation defined by laser scanning direction, and precise CNT placement with high spatial resolutions of ≈100 nm (Figure S6, Supporting Information).

In summary, we have developed a method to incorporate a large-amount of well-aligned MWNTs into 2D/3D polymer structures via TPP lithography. The grafting of the thiol molecules onto individual MWNTs significantly enhanced the dispersion quality of the MWNTs inside the acrylate-based resin. A TPP-compatible, homogenous MTA resin with high MWNT concentrations (up to 0.2 wt%) has been developed. Multiple benefits of MWNT loading in TPP micro/nanofabrication have been experimentally confirmed, including significantly enhanced electrical conductivity and mechanical strength. Based on the highly conductive MTA composite polymers, we have successfully fabricated various microelectronic devices, including capacitors and resistors. Moreover, by combining the TPP micro/nanofabrication with a short-time thermal annealing, precise MWNT assembly of ≈100 nm spatial resolution has been achieved. Our work paves the way toward precise assembly of MWNTs into arbitrary 3D micro/nanoarchitectures, which is promising for a broad range of device applications such as 3D electronics and MEMS/NEMS.

Experimental Section

Photoresist Preparation: Homemade MTA resins were prepared by mixing acid-purified MWNTs (Cheap Tubes Inc.), 2-Benzyl-2-(dimethylamino)-4′-morpholinobutyrophenone (BDMP, Sigma Aldrich), di-trimethylolpropane tetraacrylate (Di-TMPTTA, Sartomer), and pentaerythritol tetrakis (3-mercaptopropionate) (PETMP, Sigma Aldrich). BDMP was used as the photoinitiator with a constant concentration of 1 wt% in all resins. Di-TMPTTA and PETMP were used as the acrylate monomer and thiol, respectively. Resins containing MWNTs of various concentrations (0, 0.05, 0.1, 0.15, and 0.2 wt%) were prepared. The mixtures first underwent 90 s ultrasonic agitation (agitation power: 60 W, SONIFIER SLPe Energy and Branson Ultrasonics) followed by magnetic stirring for 24 h at room temperature (VWR, Standard hot plate stirrer) and then were purified using high-speed centrifugation (30 min @ 6000 rpm, mini spin 5452, Eppendorf) to remove large MWNT aggregations from the resins. The as-prepared resins were stored in brown glass bottles and stirred continuously.

Two-Photon Polymerization: TPP fabrication was performed using a 3D laser lithography system (Nanoscribe GmbH, Photonic Professional). A fs laser (center wavelength of 780 nm, pulse width of 100 fs, repetition rate of 80 MHz, and maximum power of 150 mW) was used as the irradiation source. An oil immersion objective lens (63× and 1.4 NA) was used to focus the laser beam.

Polarized Raman Microspectroscopy: Polarized Raman microspectroscopy was conducted using a Raman microscope (Renishaw, InVia H 18415). The excitation laser beam, with a wavelength of 514.5 nm, was polarized after passing through a polarizer and focused onto a sample through an objective lens (50×, NA 0.75). The polarization direction was controlled using a half-wave plate placed between the objective lens and the polarizer. Raman scattering was collected using the same objective lens, and the polarization direction was rotated to be the same as that of the incident light. The average laser power used to produce Raman spectra was 10 mW. Raman spectra were recorded with an accumulation time of 10 s each.

Scanning Electron Microscopy (SEM): A field-emission SEM (Hitachi, S4700) with an acceleration voltage of 5–10 kV was used for the observation and analyses of the TPP-fabricated structures. A chromium layer of 5 nm thick was deposited on the samples before the SEM characterization to prevent the electric charge effect.

Nanoindentation Characterization: Nanoindentation tests were performed using a nanoindenter (Hysitron, TI 750 Ubi). The maximum load was 12 mN. A conical-shaped probe (TI-0093) with a tip radius of 3 μm was used. Working times were at 20 s for the loading and unloading processes and 5 s for holding at the maximum load to avoid creep behaviors. Multiple penetration depths from 500 to 1500 nm were tested for all of the samples to ensure reliable results unaffected by surface roughness and defects.

Supporting Information

Supporting Information is available from the Wiley Online Library or from the author.

Acknowledgements

W.X. and Y.L. contributed equally to this work. This research work was financially supported by the National Science Foundation (Grant No. CMMI 1265122) and Nebraska Center for Energy Sciences Research.

Received: November 9, 2015
Revised: November 30, 2015
Published online: January 11, 2016

[1] R. Bogue, *Sensor Rev.* **2013**, *33*, 300.
[2] W. S. Zhao, Y. F. Liu, Z. Yong, Y. Fang, W. Y. Yin, in *Electrical Design of Advanced Packaging and Systems Symposium (EDAPS)*, Nara **2013**, IEEE, p. 154.
[3] a) J. S. Rodgers, *Quantum Sens. Nanophoton. Devices II* **2005**, *5732*, 511; b) A. W. Schell, J. Kaschke, J. Fischer, R. Henze, J. Wolters, M. Wegener, O. Benson, in *2013 Conference on and International Quantum Electronics Conference Lasers and Electro-Optics Europe (Cleo Europe/IQEC)* **2013**, IEEE, Munich.
[4] a) S. Takenaga, B. Schneider, E. Erbay, M. Biselli, T. Schnitzler, M. J. Schoning, T. Wagner, *Phys. Status Solidi a: Appl. Mater. Sci.* **2015**, *212*, 1347; b) J. K. Wang, G. M. Xiong, M. M. Zhu, B. Ozyilmaz, A. H. C. Neto, N. S. Tan, C. Choong, *ACS Appl. Mater. Interfaces* **2015**, *7*, 8275; c) L. Winkless, *Mater. Today* **2015**, *18*, 246.
[5] a) M. L. Gou, X. Qu, W. Zhu, M. L. Xiang, J. Yang, K. Zhang, Y. Q. Wei, S. C. Chen, *Nat. Commun.* **2014**, *5*, 3774; b) J. H. Huang, J. Kim, N. Agrawal, A. P. Sudarson, J. E. Maxim, A. Jayaraman, V. M. Ugaz, *Adv. Mater.* **2009**, *21*, 3567.
[6] Y. Cheng, Y. Liao, K. Sugioka, in *Pacific Rim Laser Damage 2013: Optical Materials for High Power Lasers*, International Society for Optics and Photonics, Shanghai, **2013**, p. 87860C–6.

[7] a) H. Schift, *J. Vac. Sci. Technol. B* **2008**, *26*, 458; b) L. J. Guo, *Adv. Mater.* **2007**, *19*, 495.
[8] A. A. Tseng, A. Notargiacomo, T. P. Chen, *J. Vac. Sci. Technol. B* **2005**, *23*, 877.
[9] Y. N. Xia, G. M. Whitesides, *Angew. Chem. Int. Ed.* **1998**, *37*, 550.
[10] A. Spangenberg, N. Hobeika, F. Stehlin, J. Pierre Malval, F. Wieder, P. Prabhakaran, P. Baldeck, O. Sopper, *Recent Advances in Two-Photon Stereolithography*, InTech, Gunma, **2013**.
[11] a) L. Li, R. R. Gattass, E. Gershgoren, H. Hwang, J. T. Fourkas, *Science* **2009**, *324*, 910; b) G. Kumi, C. O. Yanez, K. D. Belfield, J. T. Fourkas, *Lab Chip* **2010**, *10*, 1057; c) T. Buckmann, M. Thiel, M. Kadic, R. Schittny, M. Wegener, *Nat. Commun.* **2014**, *5*, 4130.
[12] H. Ishitobi, S. Shoji, T. Hiramatsu, H. B. Sun, Z. Sekkat, S. Kawata, *Opt. Express* **2008**, *16*, 14106.
[13] Z. B. Sun, X. Z. Dong, W. Q. Chen, S. Nakanishi, X. M. Duan, S. Kawata, *Adv. Mater.* **2008**, *20*, 914.
[14] K. Masui, S. Shoji, K. Asaba, T. C. Rodgers, F. Jin, X. M. Duan, S. Kawata, *Opt. Express* **2011**, *19*, 22786.
[15] H. Xia, J. A. Wang, Y. Tian, Q. D. Chen, X. B. Du, Y. L. Zhang, Y. He, H. B. Sun, *Adv. Mater.* **2010**, *22*, 3204.
[16] Y. L. Zhang, Q. D. Chen, H. Xia, H. B. Sun, *Nano Today* **2010**, *5*, 435.
[17] B. B. Xu, H. Xia, L. G. Niu, Y. L. Zhang, K. Sun, Q. D. Chen, Y. Xu, Z. Q. Lv, Z. H. Li, H. Misawa, H. B. Sun, *Small* **2010**, *6*, 1762.
[18] L. Guo, H. Xia, H. T. Fan, Y. L. Zhang, Q. D. Chen, T. Zhang, H. B. Sun, *Opt. Lett.* **2010**, *35*, 1695.
[19] a) B. Kaehr, J. B. Shear, *Proc. Natl. Acad. Sci.* **2008**, *105*, 8850; b) Y.-L. Sun, Q. Li, S.-M. Sun, J.-C. Huang, B.-Y. Zheng, Q.-D. Chen, Z.-Z. Shao, H.-B. Sun, *Nat. Commun.* **2015**, *6*, 8612.
[20] a) E. T. Thostenson, C. Y. Li, T. W. Chou, *Compos. Sci. Technol.* **2005**, *65*, 491; b) T. Fujigaya, S. Haraguchi, T. Fukumaru, N. Nakashima, *Adv. Mater.* **2008**, *20*, 2151; c) J. N. Coleman, U. Khan, Y. K. Gun'ko, *Adv. Mater.* **2006**, *18*, 689; d) J. N. Coleman, U. Khan, W. J. Blau, Y. K. Gun'ko, *Carbon* **2006**, *44*, 1624.
[21] a) N. Grossiord, J. Loos, L. van Laake, M. Maugey, C. Zakri, C. E. Koning, A. J. Hart, *Adv. Funct. Mater.* **2008**, *18*, 3226; b) D. H. Xu, Z. G. Wang, *Polymer* **2008**, *49*, 330; c) W. H. Song, Z. Zheng, W. L. Tang, X. L. Wang, *Polymer* **2007**, *48*, 3658.
[22] T. McNally, P. Potschke, P. Halley, M. Murphy, D. Martin, S. E. J. Bell, G. P. Brennan, D. Bein, P. Lemoine, J. P. Quinn, *Polymer* **2005**, *46*, 8222.
[23] C. Park, Z. Ounaies, K. A. Watson, R. E. Crooks, J. Smith, S. E. Lowther, J. W. Connell, E. J. Siochi, J. S. Harrison, T. L. S. Clair, *Chem. Phys. Lett.* **2002**, *364*, 303.
[24] Q. C. Guo, S. Z. Xiao, A. Aumann, M. Jaeger, M. Chakif, R. Ghadiri, C. Esen, M. Y. Ma, A. Ostendorf, *J. Laser Micro/Nanoeng.* **2012**, *7*, 44.
[25] S. Ushiba, S. Shoji, K. Masui, J. Kono, S. Kawata, *Adv. Mater.* **2014**, *26*, 5653.
[26] S. Ushiba, S. Shoji, K. Masui, P. Kuray, J. Kono, S. Kawata, *Carbon* **2013**, *59*, 283.
[27] S. A. Ntim, O. Sae-Khow, C. Desai, F. A. Witzmann, S. Mitra, *J. Environ. Monitor.* **2012**, *14*, 2772.
[28] J. Li, P. C. Ma, W. S. Chow, C. K. To, B. Z. Tang, J. K. Kim, *Adv. Funct. Mater.* **2007**, *17*, 3207.
[29] L. H. Nguyen, M. Straub, M. Gu, *Adv. Funct. Mater.* **2005**, *15*, 209.
[30] a) C. Gao, Y. Z. Jin, H. Kong, R. L. D. Whitby, S. F. A. Acquah, G. Y. Chen, H. H. Qian, A. Hartschuh, S. R. P. Silva, S. Henley, P. Fearon, H. W. Kroto, D. R. M. Walton, *J. Phys. Chem. B* **2005**, *109*, 11925; b) L. Bokobza, *Polymer* **2007**, *48*, 4907.
[31] D. Baskaran, J. W. Mays, M. S. Bratcher, *Angew. Chem. Int. Ed.* **2004**, *43*, 2138.
[32] L. H. Xu, Z. P. Fang, P. A. Song, M. Peng, *Plasma Process. Polym.* **2010**, *7*, 785.
[33] A. H. Liu, I. Honma, M. Ichihara, H. S. Zhou, *Nanotechnology* **2006**, *17*, 2845.
[34] a) F. Borghese, P. Denti, R. Saija, M. A. Iati, O. M. Marago, *Phys. Rev. Lett.* **2008**, *100*, 163903; b) J. Do, M. Fedoruk, F. Jackel, J. Feldmann, *Nano Lett.* **2013**, *13*, 4164.
[35] S. Gong, Z. H. Zhu, S. A. Meguid, *Polymer* **2015**, *56*, 498.
[36] K. Kurselis, R. Kiyan, V. N. Bagratashvili, V. K. Popov, B. N. Chichkov, *Opt. Express* **2013**, *21*, 31029.
[37] a) H. Yang, B. Fu, D. A. Li, Y. Tian, Y. Chen, M. Mattila, Z. Z. Yong, R. Li, A. Hassanien, C. X. Yang, I. Tittonen, Z. Y. Ren, J. T. Bai, Q. W. Li, E. I. Kauppinen, H. Lipsanen, Z. P. Sun, *Nanoscale* **2015**, *7*, 11199; b) S. Shoji, H. Suzuki, R. P. Zaccaria, Z. Sekkat, S. Kawata, *Phys. Rev. B* **2008**, *77*, 153407.
[38] a) H. Li, K. Banerjee, IEEE Trans. Electron. Dev. **2009**, *56*, 2202; b) M. D'Amore, M. S. Sarto, A. G. D'Aloia, in *2010 IEEE International Symposium on Electromagnetic Compatibility* **2010**, IEEE, Ft Lauderdale, FL p. 847.